

Anisotropy in Nucleation and Growth of Two-Dimensional Islands during Homoepitaxy on "Hex" Reconstructed Au(100)

S. Günther,¹ E. Kopatzki,¹ M. C. Bartelt,² J. W. Evans,³ and R. J. Behm¹

¹*Abteilung Oberflächenchemie und Katalyse, Universität Ulm, D-89069 Ulm, Germany*

²*Institute for Physical Research and Technology, Ames Laboratory, Iowa State University, Ames, Iowa 50011*

³*Department of Mathematics, Ames Laboratory, Iowa State University, Ames, Iowa 50011*

(Received 10 February 1994)

We present results of a comprehensive scanning tunneling microscopy study of the nucleation and growth of Au islands on Au(100). It is shown that the reconstruction of the substrate produces strong anisotropic effects. Rate equation analysis of the experimental flux and temperature dependence of the island density suggests: (i) a critical size of $i = 3$ for $T = 315\text{--}380$ K, but $i > 3$ above 400 K; and (ii) strongly anisotropic diffusion, preferentially parallel to the reconstruction rows (activation energy ~ 0.2 eV). We comment on energetic and kinetic aspects of the observed island shape anisotropy.

PACS numbers: 61.16.Ch, 68.55.-a

Nucleation and growth of islands during thin film deposition has been studied for decades. Traditional analyses, using mainly scanning and transmission electron microscopy, concentrated on systems where three-dimensional islands form [1]. The results were generally interpreted via rate equations. Recent revival of interest is associated with the availability of scanning tunneling microscopy (STM) [2–7] and high resolution surface sensitive diffraction techniques [8–11], which are especially suited for analyses of nucleation and growth of two-dimensional (2D) islands on atomic length scales.

Here we provide results of the first comprehensive study of anisotropic nucleation and growth in a metal-on-metal system. STM observations on the reconstructed Au(100) surface at temperatures between 315 and 435 K are analyzed quantitatively in a rate equation approach. A key component of our analysis is the demonstration that diffusion is actually strongly anisotropic for Au on Au(100). This is a consequence of the reduced symmetry of the reconstructed Au(100) surface. To this end, we must extend the traditional mean-field rate equations [1] to treat strongly anisotropic diffusion. Comparison with "exact" Monte Carlo simulation results is also used. In this system, we observe noticeable denuded zones at steps orthogonal, but not parallel, to the reconstruction rows. Analogous behavior for Si/Si(100) homoepitaxy was attributed to strongly anisotropic diffusion [2]. In our analysis we do not preclude a priori the possibility that the observed anisotropy is caused by different sticking coefficients (anisotropic bonding) at differently oriented step edges. Instead we examine data for the dependence of the average density of islands N_x on the deposition flux R and substrate temperature T at fixed submonolayer coverages, thereby deducing diffusion anisotropy, the probable values of the critical island size i , at and above room temperature, as well as estimates of the binding energy of critical islands and the energy barrier for isolated adatom diffusion.

The experiments were performed in a UHV system with standard facilities for sample preparation and characterization and a pocket-size STM (base pressure 6×10^{-9} Pa). Final annealing of the sample was at 970 K for 2 h. More experimental details are given in Ref. [12]. Au films were evaporated from a resistively heated tungsten basket, with no detectable rise in pressure during film deposition, using flux rates between 0.001 and 1.5 monolayers (ML)/min. The sample temperature, which could not be measured directly, was determined by calibrating the current of the heating filament against the equilibrium temperature of a dummy sample, which was contacted with a thermocouple. Systematic errors in the temperature values could be as high as ± 15 K. STM images were acquired at currents between 0.1 and 1 nA, and voltages from -200 to -800 mV. They are displayed in a grey scale representation, with darker regions corresponding to lower levels.

Typical STM images of low coverage Au films are reproduced in Fig. 1. They all resolve the characteristic row modulation of the "hex" reconstructed surface. It originates from the misfit between the more densely packed quasihexagonal topmost layer and the square bulk lattice, which in a simple picture leads to a packing of six topmost layer atoms per five bulk lattice spacings in one lattice direction. Apart from a possible slight rotation of the topmost layer, the rows are approximately oriented along one of the close-packed lattice directions [13]. In Fig. 1, this surface is covered by near-rectangular islands of monatomic height, equally distributed on the terraces. Denuded zones are found in the vicinity of step edges on both the upper and lower terrace side, as had been observed for various other growth systems, e.g., Ni/Ni(100) homoepitaxy [12]. These are associated with a reduced adatom density in the vicinity of steps due to condensation of lower terrace Au adatoms at the ascending step or due to downward interlayer transport of upper terrace adatoms to the lower terrace. Figures 1(a) and 1(b) illustrate the striking effect of the step direction with respect to that

of the reconstruction rows on the width of the denuded zone. In Fig. 1(a), with the step oriented along the rows, there is practically no island depletion visible on either of the adjoining terraces, while in Fig. 1(b), with the step orthogonal to the rows, the depletion zone is about 200 Å wide, at identical coverages and deposition conditions. Both the different widths of the denuded zones as well as the rectangular shape of the Au islands are clear evidence of anisotropy effects in nucleation and growth of the 2D Au islands, without, however, allowing a unique identification of the underlying atomistic origin (see above).

Figures 1(c) and 1(d) illustrate the dependence of the density of (stable) islands N_x on the deposition flux R at 315 K and a coverage of 0.2 ML. The surface in Fig. 1(c), corresponding to $R = 0.5$ ML/min, exhibits an island density of $N_x = 4.4 \times 10^{11}/\text{cm}^2$. Island widths are typically below 30 Å, and lengths (of the long edge) range from 100 to 150 Å. At $R = 0.005$ ML/min, the island density is much lower, $N_x = 8.8 \times 10^{10}/\text{cm}^2$ [Fig. 1(d)]. Furthermore, islands now have a much higher aspect ratio with widths of less than 80 Å and lengths around 700 Å. The same trend, of decreasing island density and increasing island size and aspect ratio, is observed with increasing substrate temperature (at fixed R). These trends are discussed below.

For a quantitative analysis, the values of the island density, N_x , were determined averaging over several STM images. We find that the island density saturates rapidly with increasing coverage θ (it is nearly constant above 0.01 ML), and consistently the average island size increases linearly with θ (up to 0.2 ML). Figure 2 shows the island density N_x versus the deposition flux, at 315 K. It reveals scaling behavior characteristic of that predicted by nucleation theories [1,14], specifically $N_x \propto R^{0.37 \pm 0.03}$. The temperature dependence of the island density for a given flux rate ($R = 0.5$ ML/min) is shown in Fig. 3. We find an exponential, Arrhenius-type behavior with different exponents in the temperature ranges $315 < T < 380$ K and $400 < T < 435$ K. In the lower temperature regime one has $\ln N_x \sim (-0.17 \text{ eV})/k_B T$, and in the higher one, $\ln N_x \sim (-0.50 \text{ eV})/k_B T$, with $k_B T$ in eV. Below we interpret this transition in the Arrhenius slope as a change in critical size.

The above behavior can be analyzed via a mean-field rate equation theory [1], where one assumes the existence of a "sharp" critical size i above which islands are stable, i.e., they cannot dissociate. (In general, i is expected to depend on T). It is, however, necessary to extend the traditional theory for isotropic diffusion [1] to the strongly anisotropic case relevant here. This is described in Ref. [14], using results from 1D random walk theory

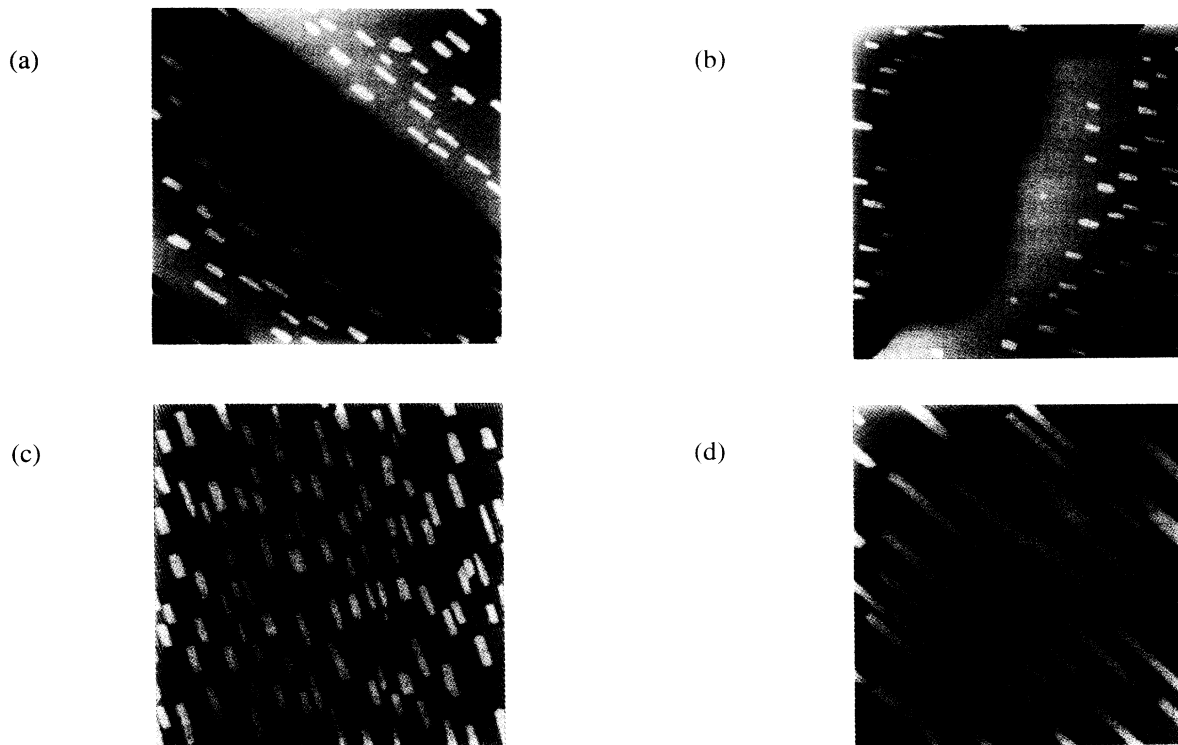


FIG. 1. Large scale STM images of submonolayer Au films on Au(100) ($1500 \text{ \AA} \times 1500 \text{ \AA}$). (a) and (b) show the different widths of the denuded zones along step edges parallel (a) and perpendicular (b) to the direction of the reconstruction rows ($R = 0.5$ ML/min, $T = 315$ K, and $\theta = 0.1$ ML). (c) and (d) show the variation in island density at different deposition fluxes but constant temperature and coverage, obtained with a flux of 0.5 ML/min (c) and 0.005 ML/min (d), respectively ($T = 315$ K, $\theta = 0.2$ ML).

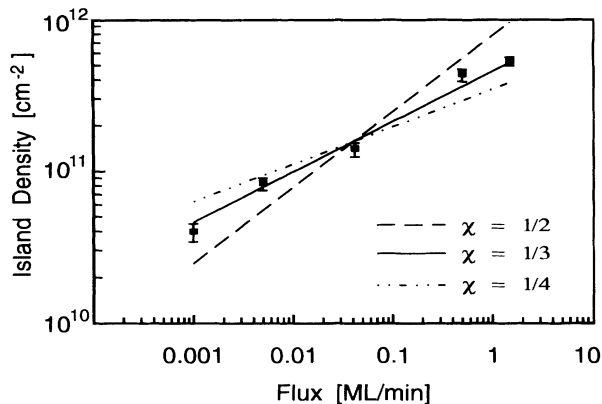


FIG. 2. Mean island density N_x as a function of the flux rate R from 10^{-3} to 1.5 ML/min, at 315 K and $\theta = 0.2$ ML. Linear regression yields a slope of $\chi = 0.37 \pm 0.03$. To illustrate the significance of the data we have included lines with $\chi = \frac{1}{2}$ ($\frac{1}{3}$) [$\chi = \frac{1}{2}$ (1) for isotropic diffusion] and $\chi = \frac{1}{4}$ (corresponding to $i = 1$ for strongly anisotropic diffusion).

to determine lifetimes for diffusing adatoms. These rate equations reveal a very short transient regime where the isolated adatom density N_1 , builds up, followed by a steady-state regime where the gain in isolated adatoms due to deposition is roughly balanced by their loss (primarily) due to aggregation with stable islands. The latter is the experimentally relevant regime. Let $h = \nu \exp(-E_d/k_B T)$ denote the hop rate for isolated adatoms, and E_i the binding energy for critical clusters. Then one finds for N_x scaling of the form

$$N_x \sim (R/\nu)^\chi \exp[\chi(E_d + E_i/i)/k_B T], \quad (1)$$

where $\chi = i/(i+2)$, if diffusion is isotropic, and $\chi = i/(2i+2)$, for strongly anisotropic (1D) diffusion. The latter relation holds for $N_1 \ll N_x$, which always applies for our system [14]. In the analysis below of the two temperature regimes in Fig. 3, with $R = 0.5$ ML/min and $\theta \approx 0.2$ ML, we choose a vibrational prefactor for h satisfying $z\nu = 8 \times 10^{12}/s$, where z is the number of possible directions for adatom hopping.

At 315 K, the experimental value of the exponent $\chi = 0.37 \pm 0.03$ is at a first view consistent with isotropic diffusion with $i = 1$. [Actually, the effective exponents found in the simulation or rate equation analysis are always below but within 90%–95% of the asymptotic value mentioned above.] Since χ increases with i , and for $i = 2$ one already has $\chi = \frac{1}{2}$, isotropic diffusion with $i > 1$ is definitely ruled out (see Fig. 2). If indeed $i = 1$ and diffusion is isotropic in this temperature range, then bonding of adatoms at terrace and island edges must be anisotropic to explain the observation of different widths of denuded zones. This does not affect the scaling of the island density with R or T . From our data an activation barrier for adatom hopping of $E_d \approx 0.5$ eV is deduced. However, simulations (and rate equations) with corresponding values of R and h at $T = 315$ K

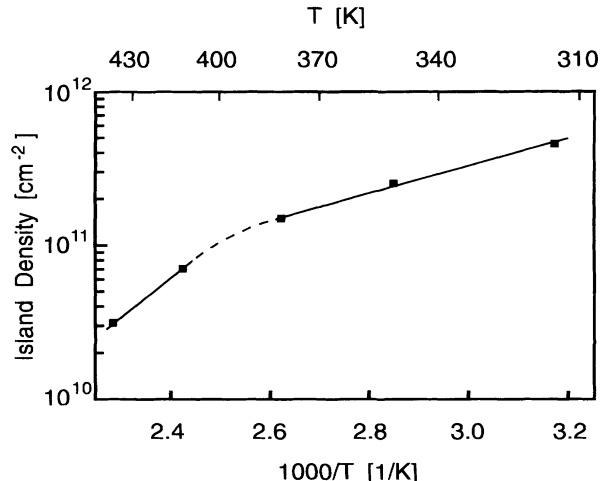


FIG. 3. Arrhenius plot of the temperature dependence of the mean island density N_x in the temperature range $315 < T < 435$ K, at fixed coverage, $\theta = 0.2$ ML ($R = 0.5$ ML/min). The error bars are about the size of the symbols.

predict a value for N_x which is 7–10 times larger than the experimental value of $N_x = 4.4 \times 10^{11}/\text{cm}^2$ (or $3.7 \times 10^{-4}/\text{site}$). These simulations [14] assume rapid restructuring of islands to compact (near square) shape, and sticking probability of unity for aggregation and nucleation, so the island density at fixed θ is determined entirely by h/R . Incorporating anisotropic bonding would increase the discrepancy with the experiment, since island growth is then further hindered relative to nucleation. The experimental value for the island density could only be matched by increasing ν by several orders of magnitude, from $\sim 10^{12}/s$ to $10^{16}/s$ (which is unrealistically high), or by inhibiting nucleation by a large factor of $\sim 10^5$ (but there is no evidence for, e.g., substrate-mediated adatom repulsion, which might produce such an effect). From these considerations, together with the observation that the shape of the experimental island size distribution disagrees with that obtained from simulations, we rule out isotropic diffusion with $i = 1$.

Next we consider the case of strongly anisotropic diffusion (which does not rule out anisotropy in bonding). Here a critical island size of $i = 1$ is excluded since the predicted $\chi = \frac{1}{4}$ is too low. So we focus on the cases $i \geq 2$. The experimental value of $\chi = 0.37 \pm 0.03$ is consistent with $i = 2-6$, noting that χ varies slowly with i . To determine system parameters, we use the full rate equations, rather than the above asymptotic formula for N_x , and demand that they both recover the experimental value for N_x at 315 K, while fitting the Arrhenius behavior, as well as reproduce the observed R dependence of N_x . We obtain the best fit for $i = 3$, with $E_d \approx 0.2$ eV and a trimer binding energy of $E_3 \approx 0.6$ eV. Unfortunately this pair of energies is not unique: values of, e.g., 0.15 or 0.25 eV for E_d , and of 0.7 or 0.5 eV for E_3 , respectively, are also consistent with the

experimental Arrhenius slope and recover the experimental N_x value. Higher values for E_3 not only require unreasonably low values to obtain N_x , but also get a progressively poorer agreement with the N_x Arrhenius slope. The E_3 values derived here are much lower than the value of 1.27 eV ($= 2 \times$ nearest neighbor bond energy of 3.81/6 eV) derived from the cohesive bulk energy of 3.81 eV. But this is expected from field ion microscopy observations [15], and from first principles [16] and simpler calculations (molecular dynamics–Monte Carlo corrected effective medium predicts $E_3 \approx 0.9$ eV [17]). Previous theoretical estimates [18,19] of $E_d \approx 0.6$ –0.8 eV for Au/Au(100) on the other side were unreliable since the reconstruction of the surface was not included or produced for the potentials used [18].

We also considered the fit of the data with a model involving diffusion with finite anisotropy. Assuming anisotropy ratios of 100–1000:1, the experimental data can be fitted with slightly higher E_d and/or E_i .

At temperatures around 390 K the slope of $\ln N_x$ versus $1/T$ gradually changes, which we attribute to a crossover to higher i in the region of $400 < T < 435$ K. Assuming that diffusion is still strongly anisotropic, we select possible values for i demanding that they allow matching of the experimental values of $N_x = 3.0 \times 10^{10}/\text{cm}^2$ at 435 K, and of the Arrhenius slope in this region. Using the estimate of $E_d \approx 0.2$ eV from above, and cluster binding energies, E_i , consistent with $E_3 \approx 0.6$ eV, we find that $i = 5$ gives marginally the best fit. However, without data for the flux dependence of the island density in this temperature region, one cannot clearly discriminate from a range of possible values $4 \leq i \leq 9$.

Refinements to our model will be required to match finer details such as the full island size distribution. For example, certain islands of more than 4 atoms might be unstable for $315 < T < 380$ K, nucleation might be restricted to certain sites, and diffusion might be restricted to strips rather than being truly one dimensional. However, we do not expect these refinements to change the basic scaling behavior in (1), or our general conclusions.

Finally we want to comment on the rectangular island shapes. Anisotropic shapes may arise from different binding energies for Au adatoms at different island edges due to the reconstruction, i.e., a thermodynamic effect, or by kinetic effects due to restricted mobilities along the island edges. We believe that the physical origin of these rectangular shapes is thermodynamic, specifically, due to anisotropic energies for binding to island edges. However, the islands are not shape equilibrated, having island aspect ratios lower than the equilibrium values as a result of kinetically limited transport of edge adatoms from the long to the short edges. This interpretation is consistent with the observation that the mean island aspect ratio A increases with decreasing deposition flux, or increasing temperature. For example, at fixed $\theta = 0.2$ ML, Figs. 1(c) and 1(d) show that A increases from about 3 to 8 as R decreases from 0.5

to 0.005 ML/min (at fixed $T = 315$ K), and we also find that $A \approx 10^2 \exp[(-0.1 \text{ eV})/k_B T]$ increases from about 3 to 7 as T increases from 315 to 435 K (at fixed $R = 0.5$ ML/min). Furthermore, other more subtle effects may influence the island shape, e.g., a possible quantization of the island width caused by the reconstruction.

In conclusion, we have shown by quantitative analysis of STM images that the nucleation and growth of 2D islands during homoepitaxy on Au(100) are controlled by strong anisotropic effects. A critical size of $i = 3$ at room temperature, which increases above 390 K, strongly anisotropic diffusion, with a barrier for adatom hopping along the reconstruction rows of about 0.2 eV, and a trimer binding energy of about 0.6 eV are inferred from the temperature and flux dependence of the mean island density. The rectangular island shapes and the increasing aspect ratio for higher temperatures suggest strongly anisotropic bonding energies and restricted edge diffusion. The origin of these anisotropy effects is sought in the “hex” reconstruction of the surface.

We gratefully acknowledge financial support from IBM Corporation within the Shared University Research (SUR) program (Contract No. 0861). The work of M. C. B. and J. W. E. was supported by NSF Grant No. CHE 9317660, and IPRT (ISU). It was performed at Ames Laboratory which is operated by Iowa State University under Contract No. W-7405-Eng-82.

- [1] J. A. Venables, G. D. Spiller, and M. Hanbücken, Rep. Prog. Phys. **47**, 399 (1984).
- [2] Y.-W. Mo *et al.*, Phys. Rev. Lett. **66**, 1998 (1991).
- [3] R. Q. Hwang *et al.*, Phys. Rev. Lett. **67**, 3279 (1991).
- [4] C. Günther *et al.*, Ber. Bunsenges. Phys. Chem. **97**, 522 (1993).
- [5] M. Bott, Th. Michely, and G. Comsa, Surf. Sci. **272**, 161 (1992).
- [6] J. A. Stroscio, D. T. Pierce, and R. A. Dragoset, Phys. Rev. Lett. **70**, 3615 (1993).
- [7] Th. Michely *et al.*, Phys. Rev. Lett. **70**, 3943 (1993).
- [8] R. Kunkel *et al.*, Phys. Rev. Lett. **65**, 733 (1990).
- [9] H.-J. Ernst, F. Fabre, and J. Lapujoulade, Phys. Rev. B **46**, 1929 (1992).
- [10] M. Henzler, Surf. Sci. **298**, 369 (1993).
- [11] G. L. Nyberg, M. T. Kief, and W. F. Egelhoff, Phys. Rev. B **48**, 14509 (1993).
- [12] E. Kopatzki, S. Günther, and R. J. Behm, Surf. Sci. **284**, 154 (1993).
- [13] M. A. van Hove *et al.*, Surf. Sci. **103**, 189 (1981); S. G. J. Mochrie *et al.*, Phys. Rev. Lett. **64**, 2925 (1990).
- [14] J. W. Evans and M. C. Bartelt, J. Vac. Sci. Technol. A **12**, 1800 (1994); M. C. Bartelt and J. W. Evans, Surf. Sci. **298**, 421 (1993).
- [15] T. T. Tsong and R. Casanova, Phys. Rev. B **24**, 3063 (1981).
- [16] P. J. Feibelman, Phys. Rev. Lett. **58**, 2766 (1987).
- [17] L. S. Perkins and A. E. DePristo (private communication).
- [18] C. L. Liu *et al.*, Surf. Sci. **253**, 334 (1991).
- [19] D. E. Sanders and A. E. DePristo, Surf. Sci. **254**, 341 (1991).

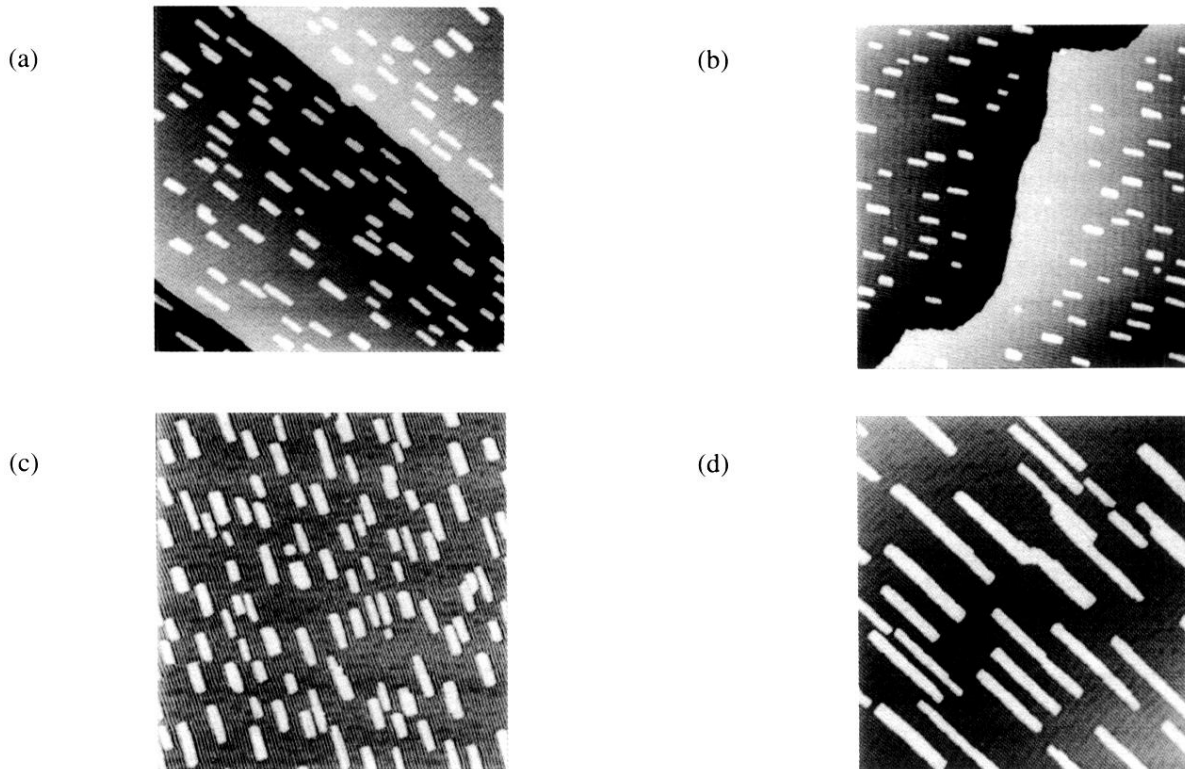


FIG. 1. Large scale STM images of submonolayer Au films on Au(100) ($1500 \text{ \AA} \times 1500 \text{ \AA}$). (a) and (b) show the different widths of the denuded zones along step edges parallel (a) and perpendicular (b) to the direction of the reconstruction rows ($R = 0.5 \text{ ML/min}$, $T = 315 \text{ K}$, and $\theta = 0.1 \text{ ML}$). (c) and (d) show the variation in island density at different deposition fluxes but constant temperature and coverage, obtained with a flux of 0.5 ML/min (c) and 0.005 ML/min (d), respectively ($T = 315 \text{ K}$, $\theta = 0.2 \text{ ML}$).